# Common mechanism for inter-annual and decadal variability in the East African long rains

**Dean P. Walker**[1], **John H. Marsham**[1,2], **Cathryn E. Birch**[1], **Adam A. Scaife**[3,4], **Declan L. Finney**[1]

[1]School of Earth and Environment, University of Leeds, Leeds, UK
[2]National Centre for Atmospheric Science, Leeds, UK
[3]Met Office Hadley Centre, Exeter, UK
[4]College of Engineering, Mathematics and Physical Sciences, University of Exeter, Exeter, UK

**Key Points:**

- East African long rains inter-annual and decadal variability have the same quantitative link to winds across the Congo and Gulf of Guinea
- Drier long rains and the corresponding zonal wind anomalies are linked to Sahelian warming on both inter-annual and decadal timescales
- The Madden-Julian Oscillation influences both the zonal winds and the long rains on inter-annual and decadal timescales

Corresponding author: Dean P. Walker, `eedpw@leeds.ac.uk`

## Abstract

The East African long rains constitute the main crop-growing season in the region. Inter-annual predictability of this season is low in comparison to the short rains, and recent decadal drying contrasts with climate projections of a wetter future (the "East African climate paradox"). Here, we show that long rains rainfall totals are strongly correlated with 700hPa zonal winds across the Congo basin and Gulf of Guinea (r=0.73). Westerly anomalies lead to more rainfall, with the same mechanism controlling rainfall variability on inter-annual and decadal timescales. On both timescales wind anomalies are linked to geopotential anomalies over the Sahel and Sahara, and warming there. Rainfall and wind are significantly correlated with the Madden-Julian Oscillation (MJO) amplitude, and around 18% of the decadal drying can be explained by MJO amplitude variability. This work shows that predictions of East African rainfall across timescales require robust prediction of both zonal winds and MJO activity.



## Plain Language Summary

East Africa has two rainfall seasons, the main season, the long rains, runs from March to May. There is currently little understanding of what controls the amount of rainfall during this season. Recent drying, causing many areas to suffer from droughts and food shortages, contrasts with climate projections of a wetter future (the "East African climate paradox"). Rainfall is found to be connected to the strength of easterly winds over the Congo basin and Gulf of Guinea, with the same mechanism controlling variability on both inter-annual and decadal timescales. From 1998 to 2011 the winds had been getting stronger, reducing rainfall over East Africa. The cause of the stronger wind is investigated, and is partly explained by relatively faster warming in the Sahel than over the Congo, whilst variation in Madden-Julian Oscillation (a large scale tropical wave) activity, explains around 18% of the decadal drying.


## 1 Introduction

Equatorial East Africa has two rainfall seasons per year, the long rains, occurring March-May (MAM), and the short rains, occurring October-December (OND). For many years, a large contrast in the predictability of the two seasons has been observed (Camberlin & Philippon, 2002; Batté & Déqué, 2011; Dutra et al., 2013; Nicholson, 2017; Walker et al., 2019). This has been attributed to the short rains being influenced by global scale modes of variability such as El Niño-Southern Oscillation (Nicholson & Entekhabi, 1986; Indeje et al., 2000), and the Indian Ocean Dipole (Saji et al., 1999; Black et al., 2003), whilst such relationships are absent during the long rains (Ogallo, 1988).

In most areas of equatorial East Africa, the long rains is the main crop growing season, generally providing greater (Camberlin & Wairoto, 1997), and more reliable (Camberlin & Philippon, 2002), rainfall amounts. However, in recent decades there has been an observed drying trend in this season (Funk et al., 2005, 2008; Liebmann et al., 2014; Maidment et al., 2015), which sharply contrasts the wetting predicted by most climate projections (Shongwe et al., 2011; Otieno & Anyah, 2013), and is often referred to as the "East African Climate Paradox" (Rowell et al., 2015). Some authors have demonstrated that the long rains decline is linked with natural decadal variability in the Pacific Ocean (Lyon, 2014; Yang et al., 2014; Bahaga et al., 2019), whilst others suggest anthropogenic factors (Williams & Funk, 2011; Funk & Hoell, 2015; Rowell et al., 2015). Meanwhile, recent work by Wainwright et al. (2019) has shown that over the Horn of Africa the observed long rains drying trend is caused by a shortening of the rainfall season, and that in more recent years, the long rains have begun to recover. Therefore the future of the long rains is still highly uncertain. Improved understanding and prediction of variability in this season on inter-annual and decadal timescales, leading to improved rainfall forecasts, would be of great benefit to the local population.

Finney et al. (2019) recently demonstrated that although the climatological wind is easterly (Figure S1a), days with westerly winds originating from over the Congo basin do occur during the long rains season, and that this is in fact true throughout the year. These events import moist air from over the Congo basin, causing convergence within the Lake Victoria basin, thereby leading to enhanced rainfall, with the record breaking 2018 long rains serving as a prime example (Kilavi et al., 2018). During MAM 2018 several westerly days occurred, linked to tropical cyclones in the Indian Ocean. Finney et al. (2019) also highlighted the role of the Madden-Julian Oscillation (MJO; Madden & Julian, 1971, 1972) influencing the formation of these tropical cyclones.

A more direct effect of MJO influence on the long rains has previously been documented by Pohl and Camberlin (2006b, 2006a). Pohl and Camberlin (2006b), using phases of the MJO defined by Wheeler and Hendon (2004), identified that phases 2 and 3 from the Wheeler-Hendon index, when the convective core is over Africa and the Indian Ocean, were linked to increased rainfall over the East African highlands. Meanwhile, Vellinga and Milton (2018) demonstrated that a greater seasonal mean amplitude of the MJO as defined by Wheeler and Hendon (2004), regardless of phase, contributed to more abundant rainfall. This is due to an asymmetric response of the rainfall to the ascent/ descent caused by specific phases.

Whilst anomalous westerly wind influence over East Africa has been regularly described qualitatively in past literature (Camberlin & Wairoto, 1997; Okoola, 1999a, 1999b; Diem et al., 2019; Nkunzimana et al., 2019), little quantitative evidence for this had been presented until the work by Finney et al. (2019). Finney et al. (2019) showed the role of absolute westerlies for East African rainfall, this work uses this understanding to demonstrate the influence of zonal wind anomalies on East African rainfall on both inter-annual and decadal timescales, demonstrating a link between long term change in the zonal winds over the Congo basin and the recently observed long rains drying trend (Section 3.1), and also investigating explanations for variability of the zonal winds (Section 3.2).

## 2 Data and Methods

The rainfall data for this study are Global Precipitation Climatology Project Version 2.3 (GPCP; Adler et al., 2003), whilst wind, geopotential height, and temperature data were obtained from European Centre for Medium-Range Weather Forecasts (ECMWF) Interim Reanalysis (ERA-Interim; Dee et al., 2011). MJO phase and amplitude data were obtained from the Bureau of Meteorology (http://www.bom.gov.au/climate/mjo), where phase and amplitude are calculated using the method outlined in Wheeler and Hendon (2004), using National Oceanic and Atmospheric Administration (NOAA) outgoing longwave radiation satellite observations (Liebmann & Smith, 1996), and National Centers for Environmental Prediction-National Centre for Atmospheric Research (NCEP-NCAR; Kalnay et al., 1996) reanalysis winds. National Aeronautics and Space Administration (NASA) Modern Era Retrospective Analysis for Research and Applications, Version 2 (MERRA-2; Gelaro et al., 2017) winds and geopotential height data were used to verify relations between ERA-Interim variables and other observations.

This study uses the period 1979-2018, matching the satellite era and earliest available data from ERA-Interim and GPCP. The region considered for rainfall is highlighted in blue in Figure 1a, and future references to East Africa will refer to this region, whilst the zonal wind index is calculated as the mean 700hPa zonal wind within 5°N to 5°S, 10°W to 30°E (brown box on Figure 1d,e).

Wet, dry, and recovery periods of the long rains, similar to those in Wainwright et al. (2019), are defined from 1979-1997 (P1), 1998-2011 (P2), and 2012-2018 (P3) respectively. Composites of the drying trend are considered using P2−P1. The wettest and driest years within the long rains are defined as years where the rainfall total is more than 0.8 standard deviations above and below the mean seasonal total over the 1979-2018 period respectively. When discussing these sets of years, this work will use DECADAL to refer to the altered Wainwright periods (P2−P1), and INTERANNUAL to refer to the driest minus wettest years.

Linear trends were calculated by regressing time series data against year of observation, and detrending was performed by removing the calculated gradient from the original data. Significance of trends were tested using the Mann-Kendall test, (Mann, 1945; Kendall, 1975), further details of which can be found in Wilks (2011).

The expected trend in rainfall, $m_{r,exp}$, due to the observed trend in wind, $m_{u,obs}$, through the mechanism with which rainfall, $r$ and wind, $u$, are related on inter-annual timescales, is given by

$$m_{r,exp} = \frac{\mathrm{d}r_d}{\mathrm{d}u_d} m_{u,obs} \tag{1}$$

where $\frac{\mathrm{d}r_d}{\mathrm{d}u_d}$ is the regression coefficient of rainfall against wind after detrending both variables, denoted by subscript $d$. If $m_{r,exp} \approx m_{r,obs}$, where $m_{r,obs}$ is the observed trend in rainfall, then this is evidence that the mechanism that links rainfall and winds on inter-annual timescales can also explain the trend in the rainfall.

Similarly, the expected change in mean rainfall between P1 and P2, $\Delta\bar{r}_{exp}$, due to the observed change in mean wind from P1 to P2, $\bar{u}_{P2} - \bar{u}_{P1}$, is given by:

$$\Delta\bar{r}_{exp} = \frac{\mathrm{d}r}{\mathrm{d}u}(\bar{u}_{P2} - \bar{u}_{P1}) \tag{2}$$

where $\frac{\mathrm{d}r}{\mathrm{d}u}$ is the gradient of the regression of rainfall against wind without detrending. In both Equation 1 and 2, variables $r$ and $u$ can be replaced by other variables.

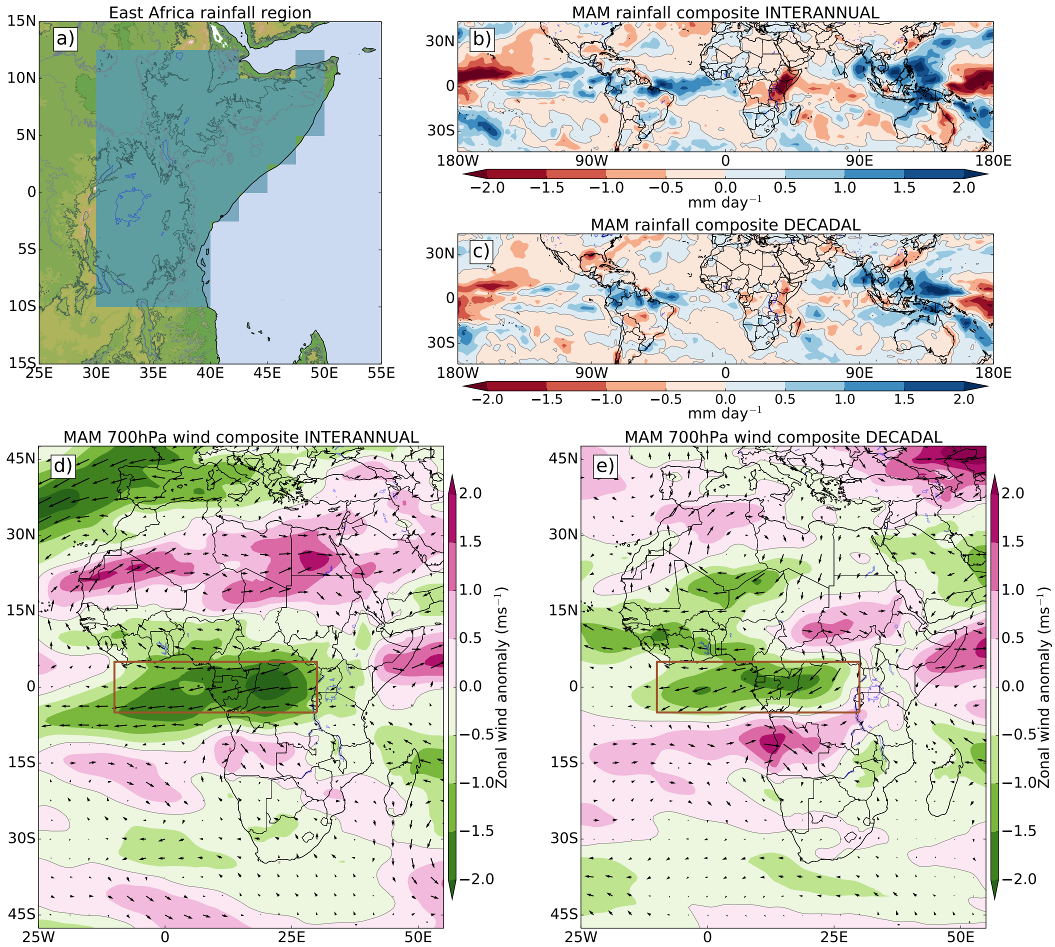


**Figure 1.** Inter-annual and decadal rainfall changes in East Africa. (a) East Africa rainfall region shaded blue, East Africa topography, colours, 500m and 1000m contours in light and dark grey. Composite of rainfall across the tropics during the long rains for (b) Driest years minus wettest years, (c) dry period minus wet period (P2−P1). Composite of 700hPa winds and zonal wind (colours) across Africa during the long rains for (d) Driest years minus wettest years, (e) Dry period minus wet period (P2−P1). Brown boxes show region used to calculate zonal wind index.

# 3 Results

## 3.1 Inter-annual and decadal variability of the long rains

Figure 1 shows rainfall anomalies over the tropics and 700hPa wind anomaly composites over Africa for INTERANNUAL and DECADAL. The 700hPa level was chosen as it is largely above the topography of East Africa, and was found to have the largest single level moisture flux, and moisture flux anomaly in the INTERANNUAL composite (Figure S1b). In Figure 1b,c a dry signal is apparent over East Africa as expected, and wet anomalies over the Maritime Continent are present, with dry anomalies over the western Pacific, in a pattern reminiscent of the Pacific 'V' discussed in Lyon and Dewitt (2012); Funk and Hoell (2015); Funk et al. (2019). In Figure 1d,e a large easterly anomaly is present over the equatorial Atlantic Ocean and Congo basin. In INTERANNUAL, this extends to the Horn of Africa where it meets a westerly anomaly from the Indian Ocean, whilst in DECADAL this easterly anomaly is also present, but only reaches as far as the orography separating the Congo basin from East Africa (repeating Figure 1d after detrending produces similar results, not shown). In both INTERANNUAL and DECADAL, the easterly anomalies appear to be linked to an anticyclonic anomaly over the Sahara desert; this level exhibits a mid-tropospheric high pressure, over the location of the summertime Saharan Heat Low (SHL), suggesting a stronger SHL in drier years (Evan et al., 2015), and which is discussed further in Section 3.2. This zonal wind anomaly (outlined by the brown box) is largely consistent with the findings of Finney et al. (2019), as an easterly anomaly in the seasonal mean is likely to contain less westerly, or weak easterly days. These results are insensitive to the reanalysis used, with similar patterns observed in equivalent MERRA-2 composites (Figure S2a,b).

Figure 2 shows the time series of the zonal wind index, and long rains seasonal rainfall anomalies. A correlation between the rainfall and zonal winds of 0.73 is found, 0.70 when detrended (both significant at the 1% level). This demonstrates the very strong connection between inter-annual variability in zonal wind and rainfall. This is again consistent in MERRA-2, with correlations of 0.81 (0.79 when detrended; Figure S2c). It is also apparent from Figure 2a that both the rainfall and zonal wind demonstrate a decreasing trend, both of which are significant at the 5% level using the Mann-Kendall trend test. Both variables show some signs of a recovery in P3, consistent with Wainwright et

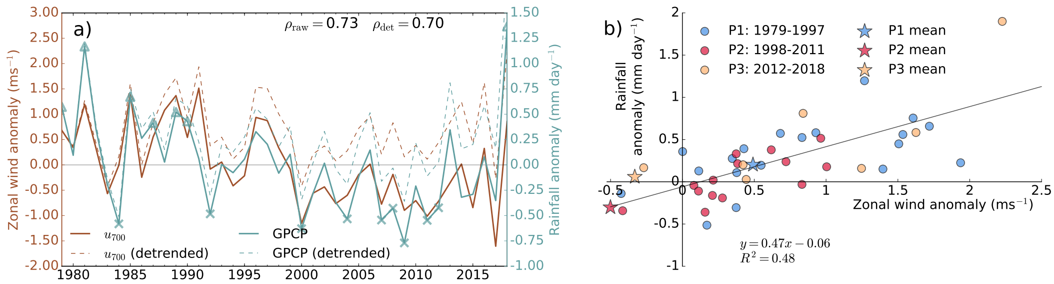


**Figure 2.** Temporal variations in East African rainfall and winds. (a) Time series of seasonal mean zonal wind anomaly (brown) and rainfall anomaly (blue) for boxes defined in Figure 1, dashed lines show time series after removing linear trends. The wet and dry years used for the INTERANNUAL composites are highlighted as triangles and crosses respectively. Correlation values of zonal winds against rainfall, before and after detrending given in top right. (b) Scatter of zonal wind anomaly against rainfall anomaly after linear detrending, coloured by P1 (blue), P2 (red), and P3 (yellow) periods. Black line is regression line fitted against the detrended scatter, with regression equation and $R^2$ value given. Coloured stars show mean anomaly of each period, with respect to 1979-2018 mean, before trend is removed.

al. (2019). This is more apparent in the rainfall than winds in Figure 2a, whilst for MERRA-2 (Figure S2c) a recovery in the zonal winds is more visible.

Figure 2b shows the scatter of rainfall against zonal wind after detrending. The linear regression equation between the two variables is $r = 0.47u - 0.06$. From this, and from the linear trend of each variable, an expected trend of rainfall due to the observed trend in the zonal winds can be calculated (Equation 1). The observed trend in zonal winds is $-0.035\pm0.009$ ms$^{-1}$year$^{-1}$, therefore the expected rainfall trend is calculated to be $-0.017\pm0.005$ mm day$^{-1}$ year$^{-1}$, whilst the observed trend in rainfall is $-0.014\pm0.006$ mm day$^{-1}$ year$^{-1}$. As this expected trend in rainfall is statistically indistinguishable from the observed trend, it is concluded that the observed decadal drying in the long rains can be largely explained by the same mechanism controlling the interannual relation between the zonal wind and rainfall. Similarly, using Equation 2 to find expected change in mean rainfall from observed change in mean zonal wind from P1 to P2 yields the result that the expected and observed change are statistically indistinguishable: $-0.47\pm0.14$ mm day$^{-1}$ expected against $-0.50\pm0.16$ mm day$^{-1}$ observed, again suggesting that the long rains trend is attributable to zonal wind changes over the Congo basin and Gulf of Guinea.

### 3.2 Drivers of variability of the zonal winds

As the main conclusion of Section 3.1 is that the zonal winds are strongly correlated with the long rains on the inter-annual timescale, and can explain the decadal drying trend, an important question is to understand what is controlling variability in these zonal winds on inter-annual and decadal timescales.

Recent work has shown the influence of the MJO amplitude on the long rains on inter-annual timescales (Pohl & Camberlin, 2006a; Vellinga & Milton, 2018). Figure 3a shows the time series of rainfall and zonal wind index alongside the February-March MJO amplitude used in Vellinga and Milton (2018). Correlation between MJO amplitude and zonal winds is 0.31, and between MJO and rainfall is 0.36 (0.40 and 0.41 respectively when detrended). These fairly weak correlations are nevertheless significant at the 5% level, and correlations between MJO and zonal wind are stronger in MERRA-2 (0.48, 0.54 when detrended). In Figure 3a, there is significantly lower (at 5% level) mean MJO amplitude during P2 than P1 and P3. The mean MJO amplitude of P2 is 1.31±0.07 whilst P1 and P3 are 1.53±0.11 and 1.70±0.09 respectively. The zonal wind index was regressed against the MJO amplitude ($a$), giving a regression equation of $u = 0.58a - 0.86$. The change in mean MJO amplitude from P1 to P2 is $-0.21\pm0.14$, giving an expected change in mean zonal wind of $-0.13\pm0.07\text{ms}^{-1}$ from Equation 2. The observed change in the zonal wind from P1 to P2 is $-0.99\pm0.26\text{ms}^{-1}$, meaning approximately 13% of the change in zonal wind can be attributed to the decrease in the amplitude of the MJO. Similarly, regressing the rainfall against the MJO amplitude leads to a regression equation of $r = 0.41a - 0.61$, giving an expected change of $-0.09\pm0.10$ mm day$^{-1}$. The observed change in mean of the rainfall from P1 to P2 is $-0.50\pm0.14$ mm day$^{-1}$, so approximately 18% of the change in rainfall can be attributed to the decrease in MJO amplitude.

Pohl and Camberlin (2006b) highlighted how different phases of the MJO influence winds around East Africa, some phases giving easterly anomalies, others westerly, so it is likely that by considering only the amplitude these opposite influences mostly cancel out, accounting for the low correlations when amplitude alone is considered. However, if the wind response to phases is asymmetric, as for rainfall, where increased descent has

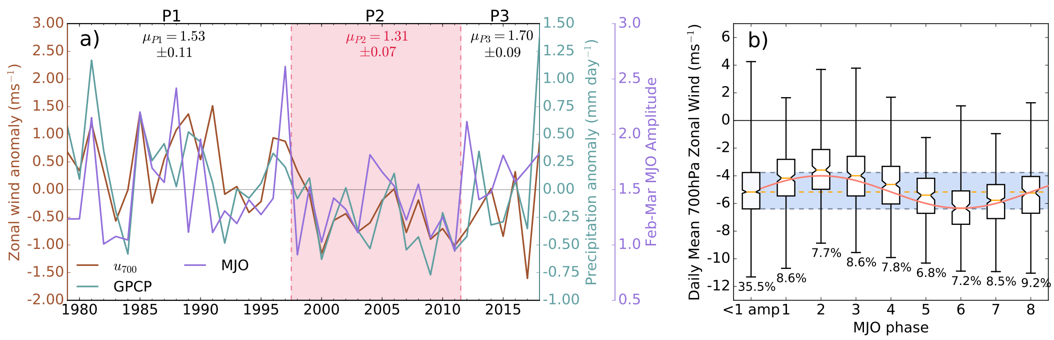


**Figure 3.** The MJO and East African rainfall. (a) Time series of zonal wind anomaly (brown) and rainfall anomaly (blue) as in Figure 2a, and February-March mean MJO amplitude (purple), means and standard errors of the MJO amplitudes during P1, P2, and P3 are given at the top, with periods separated by red dashed lines, and red shading over the dry period, P2. (b) Box plots of daily mean zonal wind separated by MJO phase, inactive days (MJO amplitude $< 1$) grouped in left box, notches on boxes show 95% confidence interval calculated from bootstrap resampling of 1000 values, numbers below min of each box show percentage of days in that phase, blue shading shows interquartile range of inactive days, orange dashed line shows median of inactive days. Pink curve shows sine wave fitted to active days assuming a mean value equal to the median of the inactive days.

less impact on rainfall than increased ascent (Vellinga & Milton, 2018), this could explain the significant correlation, providing evidence that the MJO influences inter-annual and decadal variability of the zonal winds. Alternatively it may be that the mechanism driving variability in the zonal winds also impacts MJO amplitude. The effects of different phases of the MJO on the zonal winds and rainfall are considered. Figure 3b shows box and whisker diagrams of the daily mean of the zonal wind index, separated by MJO phase, and separated into inactive days (amplitude $< 1$) and active days (amplitude $>$ 1), in MAM. If the zonal winds of the inactive days are more strongly easterly than the active days, it can be concluded that the influence of the MJO on wind is asymmetric as discussed above. To determine this, it is assumed that the converse is true: the mean winds of active and inactive days are the same. A sinusoidal wave is fitted based on this assumption, however, the wind is overall less easterly than predicted by the curve, implying that the mean winds of active and inactive days are different. In particular, the phases reducing strength of easterlies (1-4) and also phase 5, are less strongly easterly, whilst the phases increasing strength of easterlies are found to lie roughly on the curve. To confirm this, taking the mean zonal wind of all active ($-4.81\text{ms}^{-1}$), and inactive days ($-5.02\text{ms}^{-1}$), and performing a one-sided t-test, it is found that the mean zonal winds of active days are less easterly (significant at the 1% level). Despite this asymmetry, it is still possible that rather than the MJO influencing the zonal winds (or vice-versa), the correlation could result from a third process influencing both the MJO amplitude and zonal winds separately.

Whilst the MJO can explain some of the inter-annual and decadal variability of the zonal winds, the fairly weak correlation and low percentage of explained change in mean suggests other factors must be involved. Figure 4 shows dry minus wet composites of geopotential height at 700hPa (Z700), and the geopotential thickness between 700hPa and 925hPa (Z700$-$Z925), alongside 700hPa winds, for INTERANNUAL and DECADAL. In both the INTERANNUAL and DECADAL the 700hPa wind anomalies follow closely the gradients in anomaly in Z700, as expected.

There are large similarities between the composites of Z700 and geopotential thickness. In the INTERANNUAL composites (Figure 4a,b), there is a geopotential thickness anomaly over the eastern Sahel, extending over Arabia, similar to the anomaly in Z700. This area is also where both geopotential thickness and Z700 are maximal in the climatology (Figure S1c,d). Therefore, in dry years, the maxima in geopotential thick-

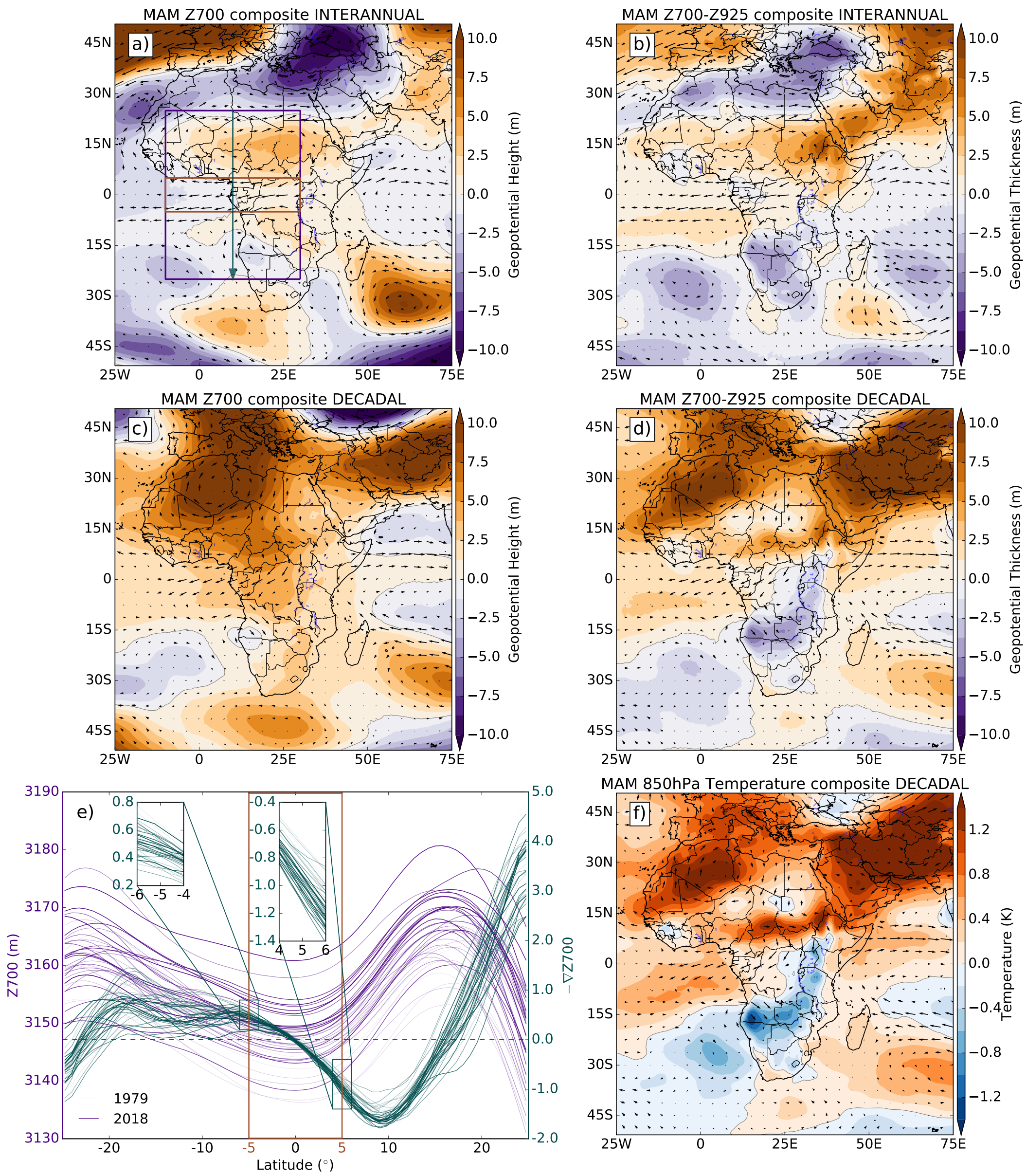


**Figure 4.** Inter-annual and decadal geopotential patterns over Africa. (a) Composites of 700hPa geopotential height and winds, (b) Composites of geopotential thickness between 700hPa and 925hPa, with 700hPa winds, for driest years minus wettest years. (c) and (d), As in a and b, but for P2−P1. (e) Transect of mean geopotential height (purple) across each latitude for the purple box shown in a, and gradient of the geopotential height (blue) multiplied by -1, following blue arrow shown in a, for each year from 1979-2018. Line thickness in order from earliest year (thinnest) to latest year (thickest). Inset boxes show geopotential gradients zoomed in to edges of zonal wind box (brown box). (f) 850hPa temperature and 700hPa winds for P2−P1.

ness and Z700 are increased, causing a larger meridional geopotential gradient from the Sahel to the Congo, consistent with increased strength of easterly winds.

In the DECADAL composites (Figure 4c,d), two large anomalies stand out over the west Sahara, and Arabian peninsula. These are the approximate locations of the summertime SHL and Arabian Heat Low (AHL). The 700hPa-925hPa geopotential thickness is a common measure of the strength of the SHL, as defined by Lavaysse et al. (2009), implying that both the SHL and AHL are stronger in drier years. However, there is also a similar pattern to the INTERANNUAL composites in the eastern Sahel, in both the geopotential thickness and Z700, with positive anomalies, reducing in magnitude from 15°N southward through the equator. This again gives an increased geopotential gradient at 700hPa, consistent with increased strength of easterly winds.

Figure 4e shows the latitudinally averaged Z700 across the purple box in Figure 4a, and latitudinal gradient of Z700 multiplied by $-1$ over this region. Thicker lines represent more recent years. An increase in Z700 across the region in more recent years is evident, with thicker lines having higher Z700. Such a trend is not apparent in the geopotential gradient, however, there is a maximum (trough) in the gradient at roughly 10°N, with more recent years displaying a stronger maximum. This causes a stronger gradient on the north side of the zonal wind box (5°N: right inset of Figure 4e) whilst at the southern edge of the box (5°S: left inset of Figure 4e) such a pattern is absent. This shows that the increased meridional geopotential gradient across the zonal wind box is related to the increased geopotential gradient to the north, from the increasingly strong maximum in the Z700 in the eastern Sahel. This is also apparent in MERRA-2 (Figure S2d).

Finally, via the hypsometric equation, the geopotential thickness between two layers is directly proportional to the mean temperature within them. Figure 4f shows the composite of 850hPa temperature for DECADAL, this is consistent with the geopotential thickness composite. Therefore, from P1 to P2, the increase in geopotential thickness is driven by a more rapidly warming eastern Sahel and west Sahara, than over the Congo basin, increasing the meridional geopotential gradient at 700hPa, with increasingly strong easterly winds over the Congo region and drier East Africa.

## 4 Discussion and Conclusions

This study has investigated the relationship between 700hPa zonal winds across the Gulf of Guinea and Congo basin, and rainfall in East Africa during the long rains. It was found that the seasonal mean 700hPa zonal wind over this area is strongly correlated with East African long rains rainfall totals (r=0.73). Considering periods similar to Wainwright et al. (2019), with a wet (P1: 1979-1997), dry (P2: 1998-2011), and recovery period (P3: 2012-2018), it was found that the same relationship is seen on decadal timescales (P2−P1), showing the importance of the zonal winds to East African climate paradox drying. Meanwhile, a recovery during P3, in agreement with Wainwright et al. (2019), is seen not only in rainfall, but also in the zonal winds. The mechanism linking the zonal winds to rainfall on inter-annual timescales is also found to quantitatively explain the long rains drying trend through the decreasing trend in the zonal winds.

The mechanism driving variability in the zonal winds was explored, with some contribution coming from the MJO amplitude, both on inter-annual and decadal timescales, with wind response to MJO by phase being subtly asymmetric, as seen for rainfall (Vellinga & Milton, 2018). There was a significantly weaker MJO amplitude during P2, accounting for 18% and 13% of the decline in rainfall and wind respectively. Meanwhile, another mechanism for the inter-annual and decadal variability was shown considering changes in geopotential gradients. For inter-annual variability, these lead to stronger easterlies in drier years due to higher geopotential height over the eastern Sahel, caused by increased warming here, strengthening the geopotential gradient. For decadal variability, a similar mechanism is present, but is also aligned to increased heating around Arabia and Sahara regions.

What has not been explored is the source of differing rates of warming between the Sahel and the Congo basin. During the study period, a decadal decline in rainfall over Arabia has been reported (Almazroui et al., 2012), excess heating during this period could be linked to a decadal trend in dust activity over the Arabian Peninsula (Yu et al., 2015), that is also causing a strengthening AHL (Solmon et al., 2015). Wainwright et al. (2019) has linked a deepening AHL to faster progression of the tropical rain-band over East Africa during the long rains, shortening the season, and Dunning et al. (2018) links a deepening SHL under climate change to a delayed return of the rain-band southwards in boreal autumn. The eastern Sahel and Arabia region has experienced a rapid, almost steplike change in temperature around the end of P1 (Almazroui et al., 2012; Attada et al., 2018; C. M. Taylor et al., 2018; Hu et al., 2019). The amplified Saharan change in temperature is linked to the observed deepening of the SHL, also responsible for the partial recovery of the Sahelian drought (Evan et al., 2015). Thus the SHL plays two key roles: affecting monsoon onset/ retreat and the latitudinal progression of the rain band (Lavaysse et al., 2009; Dunning et al., 2018), and as shown here by affecting zonal winds across central Africa, which are important for water vapour transport and East African rainfall (Finney et al., 2019). Further strengthening of the SHL is expected under climate change (Biasutti et al., 2009; Dong & Sutton, 2015), which through the above mechanisms could lead to further drying of the long rains.

Based on these results, further understanding of how relative warming rates might change in the future could provide an alternative viewpoint into the future of the long rains through changes in regional dynamics (also supported by Kent et al., 2015). For example, Giannini et al. (2018) demonstrated that in the Coupled Model Intercomparison Project phase 5 (CMIP5; K. E. Taylor et al., 2012), a mechanism consistent with wetter years shown here is present during MAM, with moisture advected away from the Congo towards East Africa, linked to a slower overturning circulation under climate change.

Whilst in the long rains, sea surface temperatures (SSTs) are less well connected to rainfall totals than in the short rains, weaker, but significant relations do exist on both inter-annual (Ogallo, 1988; Vellinga & Milton, 2018), and longer term (Williams & Funk, 2011; Liebmann et al., 2014; Bahaga et al., 2019) timescales. Therefore, understanding how the processes discussed here are influenced by SSTs could determine their predictability. Given that these zonal winds are of great importance to variability within the long rains, it should be a priority to investigate whether forecast models are able to capture this relationship. This could improve seasonal forecasting and provide useful information on the potential future of the long rains.

## Acknowledgments

This work was supported by the Natural Environment Research Council (NERC) through an industrial CASE award with the UK Met Office (grant NE/N008227/1). Marsham and Finney were supported by the HyCRISTAL project (grant NE/M02038X/1). Birch and Marsham were supported by the UK Research and Innovation as part of the Global Challenges Research Fund, grant number NE/P021077/1 (GCRF African SWIFT). Marsham was also supported by the NCAS ACREW project. Scaife was supported by the Joint DECC/Defra Met Office Hadley Centre Climate Programme (GA01101). The authors would like to thank Michael Vellinga and Dave Rowell for their helpful discussions. The GPCP data were provided by NOAA/ESRL PSD, Boulder, Colorado, USA, and the ERA-Interim Reanalysis data by ECMWF, Reading, UK. MERRA-2 was provided by the Global Modelling and Assimilation Office, NASA, USA. Daily MJO Index data were provided by the Bureau of Meteorology, Melbourne, Australia.

## References

Adler, R. F., Huffman, G. J., Chang, A., Ferraro, R., Xie, P.-P., Janowiak, J., ... Nelkin, E. (2003). The Version-2 Global Precipitation Climatology Project (GPCP) monthly precipitation analysis (1979-Present). *Journal of Hydrometeorology*, *4*(6), 1147–1167. doi: 10.1175/1525-7541(2003)004⟨1147:TVGPCP⟩2.0.CO;2

Almazroui, M., Islam, M. N., Jones, P. D., Athar, H., & Rahman, M. A. (2012). Recent climate change in the Arabian Peninsula: Seasonal rainfall and temperature climatology of Saudi Arabia for 1979-2009. *Atmospheric Research*, *111*, 29–45. doi: 10.1016/j.atmosres.2012.02.013

Attada, R., Dasari, H. P., Chowdary, J. S., Yadav, R. K., Knio, O., & Hoteit, I. (2018). Surface air temperature variability over the Arabian Peninsula and its links to circulation patterns. *International Journal of Climatology*, *39*(1), 445–464. doi: 10.1002/joc.5821

Bahaga, T. K., Fink, A. H., & Knippertz, P. (2019). Revisiting interannual to decadal teleconnections influencing seasonal rainfall in the Greater Horn of Africa during the 20th century. *International Journal of Climatology*, *39*(5), 2765–2785. doi: 10.1002/joc.5986

Batté, L., & Déqué, M. (2011). Seasonal predictions of precipitation over Africa using coupled ocean-atmosphere general circulation models: Skill of the ENSEMBLES project multimodel ensemble forecasts. *Tellus, Series A: Dynamic Meteorology and Oceanography*, *63A*(2), 283–299. doi: 10.1111/j.1600-0870.2010.00493.x

Biasutti, M., Sobel, A. H., & Camargo, S. J. (2009). The role of the Sahara low in summertime Sahel rainfall variability and change in the CMIP3 models. *Jour-*

*nal of Climate*, *22*(21), 5755–5771. doi: 10.1175/2009JCLI2969.1

Black, E., Slingo, J., & Sperber, K. R. (2003). An observational study of the relationship between excessively strong short rains in coastal East Africa and Indian Ocean SST. *Monthly Weather Review*, *131*(1), 74–94. doi: 10.1175/1520-0493(2003)131⟨0074:AOSOTR⟩2.0.CO;2

Camberlin, P., & Philippon, N. (2002). The East African March-May rainy season: associated atmospheric dynamics and predictability over the 1968-97 period. *Journal of Climate*, *15*(9), 1002–1019. doi: 10.1175/1520-0442(2002)015⟨1002:TEAMMR⟩2.0.CO;2

Camberlin, P., & Wairoto, J. G. (1997). Intraseasonal wind anomalies related to wet and dry spells during the "long" and "short" rainy seasons in Kenya. *Theoretical and Applied Climatology*, *58*(1-2), 57–69. doi: 10.1007/BF00867432

Dee, D. P., Uppala, S. M., Simmons, A. J., Berrisford, P., Poli, P., Kobayashi, S., ... Vitart, F. (2011). The ERA-Interim reanalysis: configuration and performance of the data assimilation system. *Quarterly Journal of the Royal Meteorological Society*, *137*(656), 553–597. doi: 10.1002/qj.828

Diem, J. E., Sung, H. S., Konecky, B. L., Palace, M. W., Salerno, J., & Hartter, J. (2019). Rainfall characteristics and trends and the role of Congo westerlies in the western Uganda transition zone of equatorial Africa from 1983 to 2017. *Journal of Geophysical Research: Atmospheres*, *124*, 1–18. doi: 10.1029/2019jd031243

Dong, B., & Sutton, R. (2015). Dominant role of greenhouse-gas forcing in the recovery of Sahel rainfall. *Nature Climate Change*, *5*(8), 757–760. doi: 10.1038/nclimate2664

Dunning, C. M., Black, E., & Allan, R. P. (2018). Later wet seasons with more intense rainfall over Africa under future climate change. *Journal of Climate*, *31*(23), 9719–9738. doi: 10.1175/JCLI-D-18-0102.1

Dutra, E., Magnusson, L., Wetterhall, F., Cloke, H. L., Balsamo, G., Boussetta, S., & Pappenberger, F. (2013). The 2010-2011 drought in the Horn of Africa in ECMWF reanalysis and seasonal forecast products. *International Journal of Climatology*, *33*(7), 1720–1729. doi: 10.1002/joc.3545

Evan, A. T., Flamant, C., Lavaysse, C., Kocha, C., & Saci, A. (2015). Water vapor-forced greenhouse warming over the Sahara desert and the recent recovery from the Sahelian drought. *Journal of Climate*, *28*(1), 108–123. doi: 10.1175/JCLI-D-14-00039.1

Finney, D. L., Marsham, J. H., Walker, D. P., Birch, C. E., Woodhams, B. J., Jackson, L. S., & Hardy, S. (2019). The effect of westerlies on East African rainfall and the associated role of tropical cyclones and the Madden-Julian Oscillation. *Quarterly Journal of the Royal Meteorological Society*. doi: 10.1002/qj.3698

Funk, C. C., Dettinger, M. D., Michaelsen, J. C., Verdin, J. P., Brown, M. E., Barlow, M., & Hoell, A. (2008). Warming of the Indian Ocean threatens eastern and southern African food security but could be mitigated by agricultural development. *Proceedings of the National Academy of Sciences*, *105*(32), 11081–11086. doi: 10.1073/pnas.0708196105

Funk, C. C., & Hoell, A. (2015). The leading mode of observed and CMIP5 ENSO-residual sea surface temperatures and associated changes in indo-pacific climate. *Journal of Climate*, *28*(11), 4309–4329. doi: 10.1175/JCLI-D-14-00334.1

Funk, C. C., Pedreros, D., Nicholson, S., Hoell, A., Korecha, D., Galu, G., … Pomposi, C. (2019). Examining the Potential Contributions of Extreme Western V Sea Surface Temperatures to the 2017 MarchJune East African Drought. *Bulletin of the American Meteorological Society*, *100*(1), S55–S60. doi: 10.1175/BAMS-D-18-0108.1

Funk, C. C., Senay, G., Asfaw, A., & Verdin, J. (2005). Recent drought tendencies in Ethiopia and equatorial-subtropical eastern Africa. *FEWS NET Special Report*.

Gelaro, R., McCarty, W., Suárez, M. J., Todling, R., Molod, A., Takacs, L., … Zhao, B. (2017). The modern-era retrospective analysis for research and applications, version 2 (MERRA-2). *Journal of Climate*, *30*(14), 5419–5454. doi: 10.1175/JCLI-D-16-0758.1

Giannini, A., Lyon, B., Seager, R., & Vigaud, N. (2018). Dynamical and thermodynamic elements of modeled climate change at the East African margin of convection. *Geophysical Research Letters*, *45*(2), 992–1000. doi: 10.1002/2017GL075486

Hu, L., Luo, J.-J., Huang, G., & Wheeler, M. C. (2019). Synoptic features responsible for heat waves in Central-Africa, a region with strong multi-decadal trend.

*Journal of Climate*, *32*(22), 7951–7970. doi: 10.1175/jcli-d-18-0807.1

Indeje, M., Semazzi, F. H., & Ogallo, L. J. (2000). ENSO signals in East African rainfall seasons. *International Journal of Climatology*, *20*(1), 19–46. doi: 10.1002/(SICI)1097-0088(200001)20:1⟨19::AID-JOC449⟩3.0.CO;2-0

Kalnay, E., Kanamitsu, M., Kistler, R., Collins, W., Deaven, D., Gandin, L., … Joseph, D. (1996). The NCEP / NCAR 40-Year Reanalysis Project. *Bulletin of the American Meteorological Society*, *77*(3), 437–472. doi: 10.1175/1520-0477(1996)077⟨0437:TNYRP⟩2.0.CO;2

Kendall, M. G. (1975). *Rank Correlation Methods* (4th ed.). London: Charles Griffin.

Kent, C., Chadwick, R., & Rowell, D. P. (2015). Understanding uncertainties in future projections of seasonal tropical precipitation. *Journal of Climate*, *28*(11), 4390–4413. doi: 10.1175/JCLI-D-14-00613.1

Kilavi, M., MacLeod, D., Ambani, M., Robbins, J., Dankers, R., Graham, R., … Todd, M. C. (2018). Extreme rainfall and flooding over central Kenya including Nairobi city during the long-rains season 2018: Causes, predictability, and potential for early warning and actions. *Atmosphere*, *9*(12). doi: 10.3390/atmos9120472

Lavaysse, C., Flamant, C., Janicot, S., Parker, D. J., Lafore, J. P., Sultan, B., & Pelon, J. (2009). Seasonal evolution of the West African heat low: A climatological perspective. *Climate Dynamics*, *33*(2-3), 313–330. doi: 10.1007/s00382-009-0553-4

Liebmann, B., Hoerling, M. P., Funk, C. C., Bladé, I., Dole, R. M., Allured, D., … Eischeid, J. K. (2014). Understanding recent eastern Horn of Africa rainfall variability and change. *Journal of Climate*, *27*(23), 8630–8645. doi: 10.1175/JCLI-D-13-00714.1

Liebmann, B., & Smith, C. A. (1996). Description of a complete (interpolated) outgoing longwave radiation dataset. *Bulletin of the American Meteorological Society*, *77*(6), 1275–1277.

Lyon, B. (2014). Seasonal drought in the Greater Horn of Africa and its recent increase during the March-May long rains. *Journal of Climate*, *27*(21), 7953–7975. doi: 10.1175/JCLI-D-13-00459.1

Lyon, B., & Dewitt, D. G. (2012). A recent and abrupt decline in the East

African long rains. *Geophysical Research Letters*, *39*(2), L02702. doi: 10.1029/2011GL050337

Madden, R. A., & Julian, P. R. (1971). Detection of a 40-50 day oscillation in the zonal wind in the tropical Pacific. *Journal of the Atmospheric Sciences*, *28*(5), 702–708. doi: 10.1175/1520-0469(1971)028⟨0702:DOADOI⟩2.0.CO;2

Madden, R. A., & Julian, P. R. (1972). Description of global-scale circulation cells in the tropics with a 40-50 day period. *Journal of the Atmospheric Sciences*, *29*(6), 1109–1123. doi: 10.1175/1520-0469(1972)029⟨1109:DOGSCC⟩2.0.CO;2

Maidment, R. I., Allan, R. P., & Black, E. (2015). Recent observed and simulated changes in precipitation over Africa. *Geophysical Research Letters*, *42*(19), 1–10. doi: 10.1002/2015GL065765

Mann, H. B. (1945). Nonparametric tests against trend. *Econometrica*, *13*(3), 245–259.

Nicholson, S. E. (2017). Climate and climatic variability of rainfall over eastern Africa. *Reviews of Geophysics*, *55*(3), 590–635. doi: 10.1002/2016RG000544

Nicholson, S. E., & Entekhabi, D. (1986). The quasi-periodic behavior of rainfall variability in Africa and its relationship to the southern oscillation. *Archives for Meteorology, Geophysics, and Bioclimatology Series A*, *34*(3-4), 311–348. doi: 10.1007/BF02257765

Nkunzimana, A., Bi, S., Jiang, T., Wu, W., & Abro, M. I. (2019). Spatiotemporal variation of rainfall and occurrence of extreme events over Burundi during 1960 to 2010. *Arabian Journal of Geosciences*, *12*(176). doi: 10.1007/s12517-019-4335-y

Ogallo, L. J. (1988). Relationships between seasonal rainfall in East Africa and the Southern Oscillation. *Journal of Climatology*, *8*(1), 31–43. doi: 10.1002/joc.3370080104

Okoola, R. E. (1999a). A diagnostic study of the eastern Africa monsoon circulation during the northern hemisphere spring season. *International Journal of Climatology*, *19*(2), 143–168. doi: 10.1002/(SICI)1097-0088(199902)19:2⟨143::AID-JOC342⟩3.0.CO;2-U

Okoola, R. E. (1999b). Midtropospheric Circulation Patterns Associated with Extreme Dry and Wet Episodes over Equatorial Eastern Africa during the Northern Hemisphere Spring. *Journal of Applied Meteorology*, *38*(8), 1161–1169. doi:

10.1175/1520-0450(1999)038⟨1161:MCPAWE⟩2.0.CO;2

Otieno, V. O., & Anyah, R. O. (2013). CMIP5 simulated climate conditions of the Greater Horn of Africa (GHA). Part II: Projected climate. *Climate Dynamics*, *41*(7-8), 2099–2113. doi: 10.1007/s00382-013-1694-z

Pohl, B., & Camberlin, P. (2006a). Influence of the Madden-Julian Oscillation on East African rainfall. II: March-May season extremes and interannual variability. *Quarterly Journal of the Royal Meteorological Society*, *132*(621), 2541–2558. doi: 10.1256/qj.05.223

Pohl, B., & Camberlin, P. (2006b). Influence of the Madden-Julian Oscillation on East African rainfall. I: Intraseasonal variability and regional dependency. *Quarterly Journal of the Royal Meteorological Society*, *132*(621), 2521–2539. doi: 10.1256/qj.05.104

Rowell, D. P., Booth, B. B., Nicholson, S. E., & Good, P. (2015). Reconciling past and future rainfall trends over East Africa. *Journal of Climate*, *28*(24), 9768–9788. doi: 10.1175/JCLI-D-15-0140.1

Saji, N. H., Goswami, B. N., Vinayachandran, P. N., & Yamagata, T. (1999). A dipole mode in the tropical Indian ocean. *Nature*, *401*(6751), 360–363. doi: 10.1038/43854

Shongwe, M. E., van Oldenborgh, G. J., van den Hurk, B., & van Aalst, M. (2011). Projected changes in mean and extreme precipitation in Africa under global warming. Part II: East Africa. *Journal of Climate*, *24*(14), 3718–3733. doi: 10.1175/2010JCLI2883.1

Solmon, F., Nair, V. S., & Mallet, M. (2015). Increasing Arabian dust activity and the Indian summer monsoon. *Atmospheric Chemistry and Physics*, *15*(14), 8051–8064. doi: 10.5194/acp-15-8051-2015

Taylor, C. M., Fink, A. H., Klein, C., Parker, D. J., Guichard, F., Harris, P. P., & Knapp, K. R. (2018). Earlier seasonal onset of intense mesoscale convective systems in the Congo basin since 1999. *Geophysical Research Letters*, *45*(24), 13,458–13,467. doi: 10.1029/2018GL080516

Taylor, K. E., Stouffer, R. J., & Meehl, G. A. (2012). An overview of CMIP5 and the experiment design. *Bulletin of the American Meteorological Society*, *93*(4), 485–498. doi: 10.1175/BAMS-D-11-00094.1

Vellinga, M., & Milton, S. (2018). Drivers of interannual variability of the East

African 'Long Rains'. *Quarterly Journal of the Royal Meteorological Society*. doi: 10.1002/qj.3263

Wainwright, C. M., Marsham, J. H., Keane, R. J., Rowell, D. P., Finney, D. L., Black, E., & Allan, R. P. (2019). 'Eastern African Paradox' rainfall decline due to shorter not less intense Long Rains. *npj Climate and Atmospheric Science*, *2*(1), 1–9. doi: 10.1038/s41612-019-0091-7

Walker, D. P., Birch, C. E., Marsham, J. H., Scaife, A. A., Graham, R. J., & Segele, Z. T. (2019). Skill of dynamical and GHACOF consensus seasonal forecasts of East African rainfall. *Climate Dynamics*, *53*(7), 4911–4935. doi: 10.1007/s00382-019-04835-9

Wheeler, M. C., & Hendon, H. H. (2004). An all-season real-time multivariate MJO Index: Development of an index for monitoring and prediction. *Monthly Weather Review*, *132*(8), 1917–1932. doi: 10.1175/1520-0493(2004)132⟨1917:AARMMI⟩2.0.CO;2

Wilks, D. S. (2011). *Statistical Methods in the Atmospheric Sciences* (3rd ed.). Oxford: Elsevier.

Williams, A. P., & Funk, C. C. (2011). A westward extension of the warm pool leads to a westward extension of the Walker circulation, drying eastern Africa. *Climate Dynamics*, *37*(11-12), 2417–2435. doi: 10.1007/s00382-010-0984-y

Yang, W., Seager, R., Cane, M. A., & Lyon, B. (2014). The East African long rains in observations and models. *Journal of Climate*, *27*(19), 7185–7202. doi: 10.1175/JCLI-D-13-00447.1

Yu, Y., Notaro, M., Liu, Z., Wang, F., Alkolibi, F., Fadda, E., & Bakhrjy, F. (2015). Climatic controls on the interannual to decadal variability in Saudi Arabian dust activity: Toward the development of a seasonal dust prediction model. *Journal of Geophysical Research*, *120*(5), 1739–1758. doi: 10.1002/2014JD022611